Spatial structure arising from chase-escape interactions with crowding

Anudeep Surendran[1], Michael Plank[2,3] and Matthew Simpson[1]

[1]School of Mathematical Sciences, Queensland University of Technology, Brisbane, Australia

[2]School of Mathematics and Statistics, University of Canterbury, Christchurch, New Zealand

[3]Te Pūnaha Matatini, A New Zealand Centre of Research Excellence, Auckland, New Zealand

E-mail: `matthew.simpson@qut.edu.au`

13 November 2018

Abstract. Movement of individuals, mediated by localised interactions, plays a key role in numerous process including cellular biophysics and ecology. In this work, we propose an individual based model (IBM) of multispecies motility that accounts for various intraspecies and interspecies interactions in a community that is composed of an arbitrary number of distinct species. This framework allows us to explore how individual-level directional interactions scale up to generate spatial structure at the macroscale. To focus exclusively on the role of motility and directional bias in determining spatial structure, we consider conservative communities where the number of individuals in each species remains constant. We derive a mathematically tractable deterministic approximation of the IBM using an approach based on describing the dynamics of the spatial moments. An important objective of this study is to use the general IBM and spatial moment dynamics frameworks to investigate the impact of interactions in stereotypical community consisting of two distinct species. We explore how different features of interactions including interaction strength, spatial extent of interaction, and relative density of species influence the formation of the macroscale spatial patterns.

Keywords: individual-based model, spatial moment, chase, escape, attraction, repulsion.

1. Introduction

Movement and interaction among individuals are fundamental to various processes in cellular biophysics, such as directed cell movement during developmental morphogenesis (Williams and Solnica-Krezel 2017) and tissue repair (Oliveira et al. 2016). Similar movement and interactions, such as chase-escape dynamics, are important in ecological processes (Yang et al. 2014; Janosov et al. 2017). Intercellular interactions are generated by a number of factors such as the release and detection of chemical signals or mechanical forces such as cell-cell adhesion (Raz and Mahabaleshwar 2009; Tambe et al. 2011; Lambert et al. 2014). These interactions are associated with attractive or repulsive bias and influences the direction of movement of individuals (Agnew et al. 2014; Keeley et al. 2014; Binny et al. 2016a). Neighbour dependent movement and directional bias can act in unison to generate distinct spatial patterns in the cell population such as cellular aggregation (Thomas et al. 2006; Green et al. 2010). Similarly, interactions in animal herds or bird flocks can also lead to the creation of spatial patterns (Bajec and Heppner 2009; Lukeman et al. 2010). These observations suggest that individual level interactions have significant implications in the macroscale outcomes and motivate to develop mathematical models to study how the directional movement of individuals as they respond to cues from the neighbourhood, leads to the development of spatial structure.

To understand the impact of key factors relating to the motility of individuals, we focus solely on movement processes and neglect proliferation and mortality. Therefore, we consider a community with a fixed number of individuals and we explore how neighbour-dependent movement gives rise to spatial structure in that community. Prominent modelling frameworks in the context of describing movement of individuals include discrete individual based models (IBM) and continuous continuum models (Charteris and Khain 2014; Johnston et al. 2017; Gavagnin and Yates 2018). IBMs can be discrete space lattice-based or continuous space lattice free models depending on the application (Plank and Simpson 2012; Surendran et al. 2018). Lattice-based approaches restrict the movement of individuals to a discrete set of directions corresponding to adjacent lattice sites and incorporate volume exclusion (crowding) by allowing each site to be occupied by no more than a single individual (Simpson et al. 2009; Jin et al. 2018). In contrast, lattice-free models allow movement in any direction. Some lattice free models consider individuals as hard spheres of constant radius to include crowding effects (Dyson et al. 2012), while other lattice-free approaches use interaction kernels to specify the interactions between individuals (Plank and Law 2015). Employing interaction kernels can be thought of as a proxy model for non-rigid and deformable individuals since there is no absolute restriction on the location an individual occupies and the strength of interaction is weighted by a distributed interaction kernel. These considerations might be interpreted as meaning that lattice free models are more biologically relevant as they allow individuals to undergo deformation as they interact with neighbouring individuals, and this is thought to be relevant to the study of cell biology (Wolf and Friedl 2011).

Many studies that employ IBMs to analyse the motility mechanism consider individuals from a single species with identical intrinsic properties (Newman and Grima 2004; Binny et al. 2015). However, more realistic situations require consideration of movement and interaction among multiple species or multiple subpopulations. Recently, multi-species models have been developed to model movement in a community containing more than one type of individuals (Dini et al. 2018; Jin et al. 2018). Nevertheless, these models use an artificial lattice to model the movement of individuals. In this work, we consider a lattice-free IBM to describe the movement of multiple subpopulations of individuals without relying on any underlying lattice structure.

The spatial moment analysis is a continuum modelling approach that tracks the dynamics of the density of individuals, pairs, triples and so on, to describe the spatial correlation present in a population of individuals (Bolker and Pacala 1999; Law and Dieckmann 2000; Barraquand and Murrell 2013). Spatial moment analysis is advantageous over traditional mean-field analysis because spatial moments avoid assuming that individuals interact in proportion to their average density , thereby allowing for the analysis of clustered and segregated poulations (Plank and Law 2015). Spatial moment models were originally developed to understand birth-death processes without any movement in ecological communities (Bolker and Pacala 1997; Murrell and Law 2003; Law et al. 2003). However, more recent explorations suggest an important role for motility in generating spatial patterns (Binny et al. 2016a). In this work, we develop an IBM describing the movement of individuals incorporating the influence of local chase-escape (attraction-repulsion) interactions and we derive a macroscopic continuum approximation using spatial moments. To ensure our approach is realistic for biological and ecological applications, we consider a multispecies framework where the total population of individuals is composed of many, potentially distinct, species.

2. Stochastic, individual-based model

In this section, we describe our IBM framework. To keep our work as general as possible, we first consider an arbitrary number of species, and then present specific results for a stereotypical community composed of two species. These considerations are relevant to many biological situations such as the chasing and escape interactions in animal communities, interactions between different types of pigment cells in zebrafish development, and the interaction of different cell types in co-culture experimental assays (Vicsek et al. 2010; Inaba et al. 2012; Thomas et al. 2006). We construct the IBM for a spatially homogeneous environment, where the probability of finding an individual in a small region is independent of the location of that region. Hence, the IBM is relevant for communities that do not involve macroscopic density gradient of individuals (Jin et al. 2018).

2.1. General individual-based model

We consider a total of N individuals that belong to I distinct species, distributed over a continuous two-dimensional finite space, $\Omega \in \mathbb{R}^2$. At any instant of time t, the state of the IBM is characterised by the locations of individuals $\mathbf{x}_n \in \Omega$ and the types of individual $i_n \in \{1, 2, \ldots I\}$, where $n = 1, 2, \ldots, N$. The intrinsic movement rate of an individual of species i is given by m_i. We consider a continuous time Markov process where the probability of movement of an individual of species i in a short period δt is $m_i \delta t$.

An important feature of the IBM is the neighbour dependent directional bias. We suppose that the movement direction of individuals is affected by the presence of individuals from different species in the local neighbourhood. We introduce an interaction kernel, $\omega_{ij}(|\boldsymbol{\xi}|)$, to specify the neighbour-dependent directional bias acting on the reference individual, of species i, due to the presence of another individual, of species j, at a displacement $\boldsymbol{\xi}$. We choose these interaction kernels to be two-dimensional Gaussian functions, given by,

$$\omega_{ij}(|\boldsymbol{\xi}|) = \gamma_{ij} \exp\left(-\frac{|\boldsymbol{\xi}|^2}{2\sigma_{ij}^2}\right), \tag{1}$$

where γ_{ij} and $\sigma_{ij} > 0$ represent the interaction strength and the spatial extent of interaction, respectively. The sign of γ_{ij} determines the nature of the interaction. A positive γ_{ij} corresponds to repulsive interactions while negative γ_{ij} corresponds to attractive interactions. Choosing the sign of γ_{ij} allows us to simulate either an attractive or repulsive interaction, and these interactions are sometimes called chase or run interaction, respectively. The choice of a Gaussian kernel means that the influence of neighbours decays to zero at larger separation distances so that we only consider localised interactions. We define the neighbour-dependent bias as the gradient of interaction kernel, $\nabla\omega_{ij}(|\boldsymbol{\xi}|)$, so that movement events can either be directed up or down the gradient of one or more species in the population. The net bias vector for individual n is the sum of contributions from each of the neighbouring individuals, giving,

$$\widehat{\mathbf{B}}_n = \sum_{r \neq n} \nabla\omega_{i_n j_r}(|\mathbf{x}_r - \mathbf{x}_n|). \tag{2}$$

Two major factors characterise the bias vector are the strength of the bias defined as magnitude of bias vector, $|\widehat{\mathbf{B}}_n|$ and angular direction of the bias vector $\arg(\widehat{\mathbf{B}}_\mathrm{n}) \in [0, 2\pi]$. The preferred direction of movement for an individual is the angular direction of the net bias vector which allows us to bias the movement of individuals in response to the local crowdedness of the region.

Now we specify the probability density function (PDF) for the displacement that an individual of species i traverses during a movement event. The PDF is taken to be the product of two independent factors, given by,

$$\mu_i(\boldsymbol{\xi}; \widehat{\mathbf{B}}n) = u_i(|\boldsymbol{\xi}|)\, \mathrm{g}(\arg(\boldsymbol{\xi}); \widehat{\mathbf{B}}n). \tag{3}$$

The first part, $u_i(|\boldsymbol{\xi}|)$ is the PDF for the movement distance, $|\boldsymbol{\xi}|$ moved by an individual of species i. For simplicity, we treat $u_i(|\boldsymbol{\xi}|)$ as a fixed PDF that is independent of the

local environment and specified by a univariate Gaussian distribution with mean $\mu_i^{(s)}$ and standard deviation $\sigma_i^{(s)}$. The second part, $\mathrm{g}(\arg(\boldsymbol{\xi}); \widehat{\mathbf{B}}_n)$ is the PDF describing the angular direction of movement, $\arg(\boldsymbol{\xi}) \in [0, 2\pi]$, of an individual of species i due to the presence of other individuals in the neighbourhood. We choose the PDF for the angular direction of movement to be a von Mises distribution, with mean direction $\arg(\widehat{\mathbf{B}}_n)$ and concentration parameter given by $|\widehat{\mathbf{B}}_n|$,

$$\mathrm{g}(\theta; \widehat{\mathbf{B}}_n) = \frac{\exp\Big(|\widehat{\mathbf{B}}_n| \cos\Big(\theta - \arg(\widehat{\mathbf{B}}_n)\Big)\Big)}{2\pi \mathrm{I}_0(|\widehat{\mathbf{B}}_n|)}, \tag{4}$$

where I_0 is the zero order modified Bessel function. In the absence of net bias, $\widehat{\mathbf{B}}_n = \mathbf{0}$, the von Mises distribution reduces to the uniform distribution so that there is no preferred direction of movement (Binny et al. 2016b). This choice of PDF means that the likelihood of individuals moving in the preferred direction, $\arg(\widehat{\mathbf{B}}_n)$, increases with the magnitude of the bias vector. Individuals with large $|\widehat{\mathbf{B}}_n|$, are more likely to move in the direction of $\widehat{\mathbf{B}}_n$. The direction of movement of individuals with a weaker bias becomes almost uniformly distributed (Browning et al. 2017). Note that, the magnitude of $\widehat{\mathbf{B}}_n$ does not affect the distance moved. A description of the numerical method we used to implement the IBM, and computational techniques to quantify the associated spatial structure of the community are described in Appendix A.

2.2. Two species individual based model

The generalised multi-species IBM presented in Section 2.1 has applications in various scenarios involving movement and interaction of multiple types of individuals. Here, we consider a specific case of the multi-species IBM consisting of two distinct species, $I = 2$. These considerations are relevant to many ecological and biological interactions. Typically, chase-escape interactions in an animal community involve interspecies interactions that result in opposite effects on each of the species. (Vicsek 2010; Oshanin et al. 2009; Janosov et al. 2017). Another application of a two-species community is the development of skin patterns in zebrafish involving the movement of two types of pigment cells: melanophores and xanthophores. In this application melanophores tend to move away from xanthophores as xanthophores pursue the melanophores (Inaba et al. 2012). Immune cells and pathogens also undergo a similar chase and escape interaction during the phagocytosis (Janeway et al. 2005). Mutually attractive interactions between individuals of both species are seen in co-cultures of hepatocytes and stellate cells (Thomas et al. 2006). Another feature that is relevant when considering interactions between two types of cell types is the difference in cell size (Haridas et al. 2017a; Haridas et al. 2017b). To ensure that our IBM is relevant to these potential applications, we consider a community consisting of individuals from two distinct species for which the parameters in the IBM can be chosen to mimic these various applications. The intrinsic rate of movement of individuals of species 1 and 2 are m_1 and m_2, respectively.

We now introduce the bias interaction kernels that specify the contribution to the bias vector for an individual from its neighbours. The presence of two species in the community leads to four distinct type of interaction among individuals. The first two interactions correspond to the intraspecies interactions of individuals of species 1 and species 2, specified by the interaction kernels, $\omega_{11}(|\boldsymbol{\xi}|)$, and $\omega_{22}(|\boldsymbol{\xi}|)$, respectively. The remaining interspecies interactions are specified by the kernels $\omega_{12}(|\boldsymbol{\xi}|)$, and $\omega_{21}(|\boldsymbol{\xi}|)$, respectively. The sign of bias interaction strength, γ_{ij}, determines the nature of the bias. A positive interaction strength, γ_{ij}, corresponds to a repulsion of individuals of species i away from individuals of species j while negative γ_{ij} corresponds to an attraction of individuals of species i towards individuals of species j. Note that these interaction strengths do not need to be the same sign meaning that the interspecies interactions can be asymmetric, and this flexibility is part of what makes the IBM interesting. A description of bias interaction strengths relevant for two species interaction is given in Figure 1(a). Figure 1(b) shows a schematic representation of the possible direction of bias vectors of individuals of species 1 and species 2, generated as a result of the interactions with other individuals for different interaction strengths. The red and black dots represent individuals of species 1 and species 2, respectively. How the direction of the bias vector orient according to the nature of the interaction between individuals can be understood by considering the two individuals marked as I and II in Figure 1(b). Let us suppose the individual marked as I act as a reference individual and we are interested in the direction of the bias vector for this agent. When the bias interaction strength is negative, Individual I is biased towards individual II, and shown with an arrow pointed towards individual II. Conversely, when the interaction strength is positive, the arrow is pointed away from the individual II, showing a repulsive bias. Figure 1(c)-(j) show schematic representations of the neighbour-dependent bias vectors for possible scenarios involving a community consisting of two species

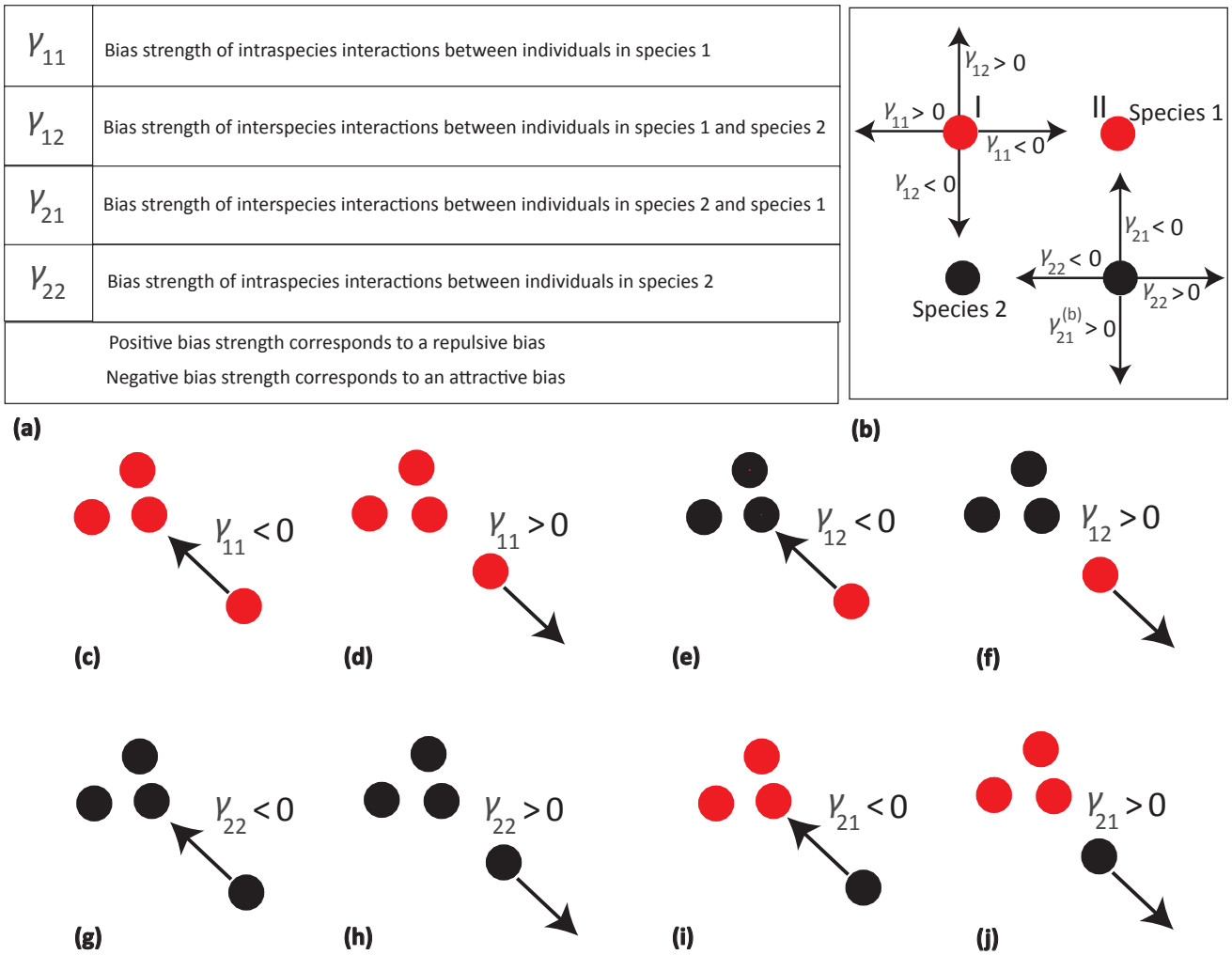

Figure 1. Schematic representation of possible interactions arising in a community consisting of two different species. **a** Table of bias strengths. **b** Schematic showing the possible directions of bias for an individual of species 1 (red) and species 2 (black) due to the presence of neighbouring individuals. **c** Attractive bias between individuals of species 1. **d** Repulsive bias between individuals of species 1. **e** Attractive bias between individuals of species 1 and 2. **f** Repulsive bias between individuals of species 1 and 2. **g** Attractive bias between individuals of species 2. **h** Repulsive bias between individuals of species 2. **i** Attractive bias between individuals of species 2 and 1. **j** Repulsive bias between individuals of species 2 and 1.

3. Spatial moment dynamics

In this section, we derive a macroscale continuum approximation of the IBM described in Section 2, by considering the dynamics of spatial moments of the individuals. First, we provide the derivation for a community consisting of an arbitrary number of species.

We use this generalised framework to explore the biologically and ecologically relevant scenario of two species community. For the homogeneous spatial point process of the kind considered in the IBM, the first spatial moment, $Z_{1,i}$ is defined as the average density of individuals of species i. Since we do not consider the proliferation and death of individuals, the first moment remains constant in time. The second spatial moment, $Z_{2,ij}(\boldsymbol{\xi}, t)$, is the average density of pairs composed of individuals of species i and species j, separated by a displacement $\boldsymbol{\xi}$. The third spatial moment, $Z_{3,ijk}(\boldsymbol{\xi}, \boldsymbol{\xi}, t)$, is defined as the average density of triplets consisting of individuals of species i, species j and species k where the individuals of species j and k are displaced by $\boldsymbol{\xi}$ and $\boldsymbol{\xi}'$, respectively from the individual of species i.

3.1. General spatial moment formulation

To derive the dynamical equation for the second spatial moment, we need to specify continuum analogues of the movement displacement PDF and bias vector. The gradient of the bias kernel, $\nabla\omega_{ij}(|\boldsymbol{\xi}|)$, gives the contribution of an individual of species j located at a displacement $\boldsymbol{\xi}$ to the bias vector of an individual of species i. The expected net bias vector for an individual of species i that is in pair with an individual of species j will depend on the contribution from another individual of species k at a displacement $\boldsymbol{\xi}$. Conditional on a pair consisting of individuals of species i and j exist at a displacement $\boldsymbol{\xi}$, the probability of an individual of species k being present at a displacement $\boldsymbol{\xi}$ is $Z_{3,ijk}(\boldsymbol{\xi}, \boldsymbol{\xi}, t)/Z_{2,ij}(\boldsymbol{\xi}, t)$. The expected net bias vector of an individual of species i, conditional on the presence of an individual of species j can be computed by multiplying the gradient of bias kernel with the conditional probability and integrating over all possible displacements, giving,

$$\mathbf{B}_{2,ij}(\boldsymbol{\xi}, t) = \sum_k \int \nabla\omega_{ik}(|\boldsymbol{\xi}'|) \frac{Z_{3,ijk}(\boldsymbol{\xi}, \boldsymbol{\xi}', t)}{Z_{2,ij}(\boldsymbol{\xi}, t)} \, \mathrm{d}\boldsymbol{\xi}' + \nabla\omega_{ij}(|\boldsymbol{\xi}|). \tag{5}$$

The additional term, $\nabla\omega_{ij}(|\boldsymbol{\xi}|)$ in Equation 5 accounts for the direct contribution of the individual of species j at displacement $\boldsymbol{\xi}$. Now we can write the PDF for the movement of an individual of species i over a displacement $\boldsymbol{\xi}'$, conditional on the presence of an individual of species j at a displacement $\boldsymbol{\xi}$ as,

$$\mu_{2,ij}(\boldsymbol{\xi}', \boldsymbol{\xi}, t) = \mu_i(\boldsymbol{\xi}'; \mathbf{B}_{2,ij}(\boldsymbol{\xi}, t)). \tag{6}$$

To derive a dynamical equation for the second spatial moment, we consider the changes in the density of pairs of individuals at a displacement $\boldsymbol{\xi}$, as a result of the movement of individuals. An existing pair of individuals at displacement $\boldsymbol{\xi}$ can be lost if one of the individuals of the pair moves. Similarly, a new pair with displacement $\boldsymbol{\xi}$ is formed when one of the individuals from an existing pair at a displacement $\boldsymbol{\xi} + \boldsymbol{\xi}$ moves a displacement $\boldsymbol{\xi}$. Accounting for these possibilities means that the time evolution of the second moment is given by,

$$\frac{\partial}{\partial t} Z_{2,ij}(\boldsymbol{\xi}, t) = -\Big(m_i + m_j\Big) Z_{2,ij}(\boldsymbol{\xi}, t) \tag{7}$$

$$+\int \Big(\mu_{2,ij}(\boldsymbol{\xi'},\boldsymbol{\xi'}+\boldsymbol{\xi},t)\,m_i\Big)Z_{2,ij}(\boldsymbol{\xi'}+\boldsymbol{\xi},t)\,\mathrm{d}\boldsymbol{\xi'}$$
$$+\int \Big(\mu_{2,ji}(\boldsymbol{\xi'},\boldsymbol{\xi'}-\boldsymbol{\xi},t)\,m_j\Big)Z_{2,ji}(\boldsymbol{\xi'}-\boldsymbol{\xi},t)\mathrm{d}\boldsymbol{\xi'}.$$

The numerical method used to solve Equation 7 is described in Appendix B. Given estimates of the first and second moments, we can describe the spatial structure of the community in terms of a pair correlation function (PCF), $C_{ij}(r)$, expressed as a function of separation distance, $r = |\boldsymbol{\xi}|$, given by,

$$C_{ij}(r) = \frac{Z_{2,ij}(\boldsymbol{\xi},t)}{Z_{1,i}\,Z_{1,j}}. \tag{8}$$

The normalisation of the second spatial moment by a factor of $Z_{1,i} \times Z_{1,j}$ in Equation 8 ensures that $C_{ij}(r) = 1$ in the absence of spatial structure. If $C_{ij}(r) > 1$, we have more pairs of an individual of species i separated by a distance r from an individual of species j than if they were in a spatially random population. We describe populations exhibiting this kind of configuration as a clustered spatial structure. On the other hand, if $C_{ij}(r) < 1$, we have fewer pairs of individuals at a separation distance r than if they were in a spatially random population and corresponding spatial configuration is known as a regular spatial pattern. The PCF is called an auto-correlation PCF when describing the density of pairs involving individuals of the same species and cross-correlation PCF when individuals are from two different species.

The dynamics of the second spatial moment depend on third spatial moment. To obtain a closed system of equations, we use a moment closure scheme to approximate third moment as a function of first and second moments (Sharkey et al. 2006; Frasca and Sharkey 2016). Different closure schemes have been used in the literature including the power-1 closure, power-2 closure and the power-3 Kirkwood superposition approximation (Murrell et al. 2004). A comparison of the performance of various closure methods for the kinds of problems we consider is summarised in Appendix C. We find that the asymmetric power-2 closure provides the best results for the range of parameters considered and so we use this closure scheme in all our computations.

3.2. Spatial moment dynamics for a community consisting of two distinct species

Now, we present the details about the spatial moment dynamics for a specific case of the generalised model presented in Section 3.1, where the community consists of individuals from two distinct species. The average densities of individuals of species 1 and species 2 are denoted by $Z_{1,1}$ and $Z_{1,2}$, respectively. Four different second spatial moments corresponds to the average density of pairs of individuals are denoted by $Z_{2,11}(\boldsymbol{\xi},t), Z_{2,12}(\boldsymbol{\xi},t), Z_{2,21}(\boldsymbol{\xi},t)$, and $Z_{2,22}(\boldsymbol{\xi},t)$, respectively.

The gradient of the bias kernel gives the contribution of individuals of both species to the bias vector of the neighbouring individual. The expected net bias vector of an individual of species 1 conditional on the presence of another individual of species 1 is

given by,

$$\mathbf{B}_{2,11}(\boldsymbol{\xi},t) = \frac{1}{Z_{2,11}(\boldsymbol{\xi},t)} \int \Big(\nabla\omega_{11}(|\boldsymbol{\xi'}|) Z_{3,111}(\boldsymbol{\xi},\boldsymbol{\xi'},t) + \nabla\omega_{12}(|\boldsymbol{\xi'}|) Z_{3,112}(\boldsymbol{\xi},\boldsymbol{\xi'},t) \Big) \, \mathrm{d}\boldsymbol{\xi'} + \nabla\omega_{11}(|\boldsymbol{\xi}|). \tag{9}$$

Similarly, the expected net bias vector of an individual of species 1 conditional on the presence of an individual of species 2 is given by,

$$\mathbf{B}_{2,12}(\boldsymbol{\xi},t) = \frac{1}{Z_{2,12}(\boldsymbol{\xi},t)} \int \Big(\nabla\omega_{11}(|\boldsymbol{\xi'}|) Z_{3,121}(\boldsymbol{\xi},\boldsymbol{\xi'},t) + \nabla\omega_{12}(|\boldsymbol{\xi'}|) Z_{3,122}(\boldsymbol{\xi},\boldsymbol{\xi'},t) \Big) \, \mathrm{d}\boldsymbol{\xi'} + \nabla\omega_{12}(|\boldsymbol{\xi}|). \tag{10}$$

The expected net bias vectors of an individual of species 2 conditional on the presence of individual of species 1 and species 2, respectively are given by,

$$\mathbf{B}_{2,21}(\boldsymbol{\xi},t) = \frac{1}{Z_{2,21}(\boldsymbol{\xi},t)} \int \Big(\nabla\omega_{21}(|\boldsymbol{\xi'}|) Z_{3,211}(\boldsymbol{\xi},\boldsymbol{\xi'},t) + \nabla\omega_{22}(|\boldsymbol{\xi'}|) Z_{3,212}(\boldsymbol{\xi},\boldsymbol{\xi'},t) \Big) \, \mathrm{d}\boldsymbol{\xi'} + \nabla\omega_{21}(|\boldsymbol{\xi}|), \tag{11}$$

$$\mathbf{B}_{2,22}(\boldsymbol{\xi},t) = \frac{1}{Z_{2,22}(\boldsymbol{\xi},t)} \int \Big(\nabla\omega_{21}(|\boldsymbol{\xi'}|) Z_{3,221}(\boldsymbol{\xi},\boldsymbol{\xi'},t) + \nabla\omega_{22}(|\boldsymbol{\xi'}|) Z_{3,222}(\boldsymbol{\xi},\boldsymbol{\xi'},t) \Big) \, \mathrm{d}\boldsymbol{\xi'} + \nabla\omega_{22}(|\boldsymbol{\xi}|). \tag{12}$$

Now we develop the equations governing the dynamics of the second moments. The equations for the density of pairs depends on the loss and gain of pairs at displacement $\boldsymbol{\xi}$. The equations governing the dynamics of second moments for the community consisting of two species are given by,

$$\begin{aligned} \frac{\partial}{\partial t} Z_{2,11}(\boldsymbol{\xi},t) = & -2\, m_1\, Z_{2,11}(\boldsymbol{\xi},t) \\ & + \int \Big(\mu_{2,11}(\boldsymbol{\xi'},\boldsymbol{\xi'}+\boldsymbol{\xi},t)\, m_1 \Big) Z_{2,11}(\boldsymbol{\xi'}+\boldsymbol{\xi},t)\, \mathrm{d}\boldsymbol{\xi'} \\ & + \int \Big(\mu_{2,11}(\boldsymbol{\xi'},\boldsymbol{\xi'}-\boldsymbol{\xi},t)\, m_1 \Big) Z_{2,11}(\boldsymbol{\xi'}-\boldsymbol{\xi},t)\, \mathrm{d}\boldsymbol{\xi'}, \end{aligned} \tag{13}$$

$$\begin{aligned} \frac{\partial}{\partial t} Z_{2,12}(\boldsymbol{\xi},t) = & -\Big(m_1 + m_2 \Big) Z_{2,12}(\boldsymbol{\xi},t) \\ & + \int \Big(\mu_{2,12}(\boldsymbol{\xi'},\boldsymbol{\xi'}+\boldsymbol{\xi},t)\, m_1 \Big) Z_{2,12}(\boldsymbol{\xi'}+\boldsymbol{\xi},t)\, \mathrm{d}\boldsymbol{\xi'} \\ & + \int \Big(\mu_{2,21}(\boldsymbol{\xi'},\boldsymbol{\xi'}-\boldsymbol{\xi},t)\, m_2 \Big) Z_{2,21}(\boldsymbol{\xi'}-\boldsymbol{\xi},t)\, \mathrm{d}\boldsymbol{\xi'}, \end{aligned} \tag{14}$$

$$\begin{aligned} \frac{\partial}{\partial t} Z_{2,21}(\boldsymbol{\xi},t) = & -\Big(m_1 + m_2 \Big) Z_{2,21}(\boldsymbol{\xi},t) \\ & + \int \Big(\mu_{2,21}(\boldsymbol{\xi'},\boldsymbol{\xi'}+\boldsymbol{\xi},t)\, m_2 \Big) Z_{2,21}(\boldsymbol{\xi'}+\boldsymbol{\xi},t)\, \mathrm{d}\boldsymbol{\xi'} \\ & + \int \Big(\mu_{2,12}(\boldsymbol{\xi'},\boldsymbol{\xi'}-\boldsymbol{\xi},t)\, m_1 \Big) Z_{2,12}(\boldsymbol{\xi'}-\boldsymbol{\xi},t)\, \mathrm{d}\boldsymbol{\xi'}, \end{aligned} \tag{15}$$

$$\frac{\partial}{\partial t} Z_{2,22}(\boldsymbol{\xi}, t) = -2\, m_2\, Z_{2,22}(\boldsymbol{\xi}, t) + \int \Big(\mu_{2,22}(\boldsymbol{\xi}', \boldsymbol{\xi}' + \boldsymbol{\xi}, t)\, m_2\Big) Z_{2,22}(\boldsymbol{\xi}' + \boldsymbol{\xi}, t)\, \mathrm{d}\boldsymbol{\xi}' + \int \Big(\mu_{2,22}(\boldsymbol{\xi}', \boldsymbol{\xi}' - \boldsymbol{\xi}, t)\, m_2\Big) Z_{2,22}(\boldsymbol{\xi}' - \boldsymbol{\xi}, t)\, \mathrm{d}\boldsymbol{\xi}'. \tag{16}$$

3.3. Summary statistics

The formation of different spatial patterns in a community is dependent on many factors such as the interaction between species and relative densities of species. To summarise the key features of the various possible combinations of spatial structure, we use a simplified metric to quantify how variations in the strength and nature of the bias interactions, as well as relative densities of species influence the formation of spatial structure. A summary statistic based on the area under the curve of the pair correlation function is one way to simply express the nature and spatial extent of the spatial structure as a single number. In this work we use,

$$A_{ij} = \int_0^R \Big(C_{ij}(r) - 1\Big)\, \mathrm{d}r, \tag{17}$$

as such a summary statistic where A_{ii} quantifies the spatial structure within species i as a function of the auto-correlation PCF $C_{ii}(r)$, whereas A_{ij} quantifies the spatial structure between species i and j as a function of the cross-correlation PCF $C_{ij}(r)$. Binny et al. (2016a) use a similar metric for describing the spatial patterns in a population consisting of individuals from a single species, but here, we use a slightly more general summary statistic since we are interested in multiple species. As we will demonstrate, plotting and comparing the various PCFs for each parameter value becomes increasingly challenging as we consider large parameter space. Under these circumstances, we find it more convenient to use A_{ij} to describe the spatial structure since it expresses the extent of the spatial structure as a single number. Our definition of A_{ij} is such that $A_{ij} > 0$ corresponds to a positive correlation between species i and species j, where individuals of species i are more likely to be located in proximity to individuals of species j. Similarly, $A_{ij} < 0$ corresponds to a negative correlation between species i and j such that individuals of species i are less likely to be located in proximity to individuals of species j. The intermediate case of $A_{ij} = 0$ corresponds to the absence of spatial structure between species i and j. We find that A_{ij} is insensitive to R when we choose R to be sufficiently large since the PCFs approaches unity for large separation distances.

4. Bias landscape

A salient feature of the IBM is the generation of directional bias due to the interactions an individual encounters within its local neighbourhood. The nature and extent of

bias experienced by an individual depend heavily on the spatial organisation of other individuals in the vicinity. The strength and spatial extent of the interactions also plays a crucial role in controlling the bias. To illuminate how these factors contribute to the generation of bias and to visualise the impact of bias on motility, we define a function that we call the *bias landscape*. The bias landscape for an individual of species i in a community composed of I distinct species is defined as $Q_i(\mathbf{x}) = \sum_{j=1}^{I} Q_{ij}(\mathbf{x})$, where $Q_{ij}(\mathbf{x})$, is the contribution to the net bias landscape of species i from the individuals in species j. Now, we focus our attention to the two-species bias landscapes. The bias landscape for an individual of species 1 is defined as,

$$Q_1(\mathbf{x}) = Q_{11}(\mathbf{x}) + Q_{12}(\mathbf{x}), \tag{18}$$

where, $Q_{11}(\mathbf{x}) = \sum_{n \in N_1} \omega_{11}(\mathbf{x}_n - \mathbf{x})$ and $Q_{12}(\mathbf{x}) = \sum_{n \in N_2} \omega_{12}(\mathbf{x}_n - \mathbf{x})$, are contributions to the net bias landscape of species 1 from the individuals in species 1 and 2, respectively. The bias landscape $Q_1(\mathbf{x})$ can be thought of as a measure of the degree of crowding experienced by an individual of species 1, located at $\mathbf{x}$. Now we can see that the net bias vector of an individual of species 1 located at $\mathbf{x}$ is $-\nabla Q_1(\mathbf{x})$, meaning the preferred direction of movement is directed down the bias landscape. The net bias vector can be written as $-\nabla Q_1(\mathbf{x}) = -\nabla Q_{11}(\mathbf{x}) - \nabla Q_{12}(\mathbf{x})$, to emphasise the combined effect of neighbouring individuals of both species 1 and species 2. The bias landscape for an individual of species 2, $Q_2(\mathbf{x})$ follows an analogous definition to that in Equation 18. Note that, the bias landscape framework is quite general that we can incorporate a range of intraspecies and interspecies interaction mechanisms that dictate the movement of individuals in a community consist of an arbitrary number of species.

The attractive or repulsive nature of bias is fundamentally related to the properties of the bias kernel that dictates the interaction between individuals. For instance, a Gaussian kernel with negative interaction strength, which is an increasing function of $|\boldsymbol{\xi}|$ creates an attractive bias. On the other hand, a Gaussian kernel with positive interaction strength, which is a decreasing function of $|\boldsymbol{\xi}|$ creates a repulsive bias. The development of bias in a sample community consisting of individuals from two distinct species, denoted by red (species 1) and black (species 2) dots is shown in Figure 2. Figure 2(a)-(b) shows the bias landscape and corresponding level curves for the intraspecies interactions of individuals of species 1. The bias landscape for the interspecies interactions of species 1 and 2 are shown in Figure 2(c). The bias vectors shown with arrows in Figure 2(a) represent the preferred direction of individuals when the contribution from individuals of species 2 is not considered. Similarly, Figure 2(d)-(e) shows the bias landscape and corresponding level curves for the intraspecies interactions of individuals of species 2. The bias landscape corresponding to the contribution of individuals of species 1 is shown in Figure 2(f). Again, the bias vectors in Figure 2(d) only accounts for contribution due to the intraspecies interaction of species 2. Now, specifying the net bias vectors for individuals of either of the species require considering intraspecies and interspecies contributions. The net bias landscape and corresponding level curves of individuals of

species 1 and species 2 are shown in Figure 2(g)-(j). Here, we see how the contribution from individuals of other species changes the net bias vector. The presence of individuals from the other species leads to a re-orientation of bias vector and often results in the enhancement or decline in the magnitude of the bias vector.

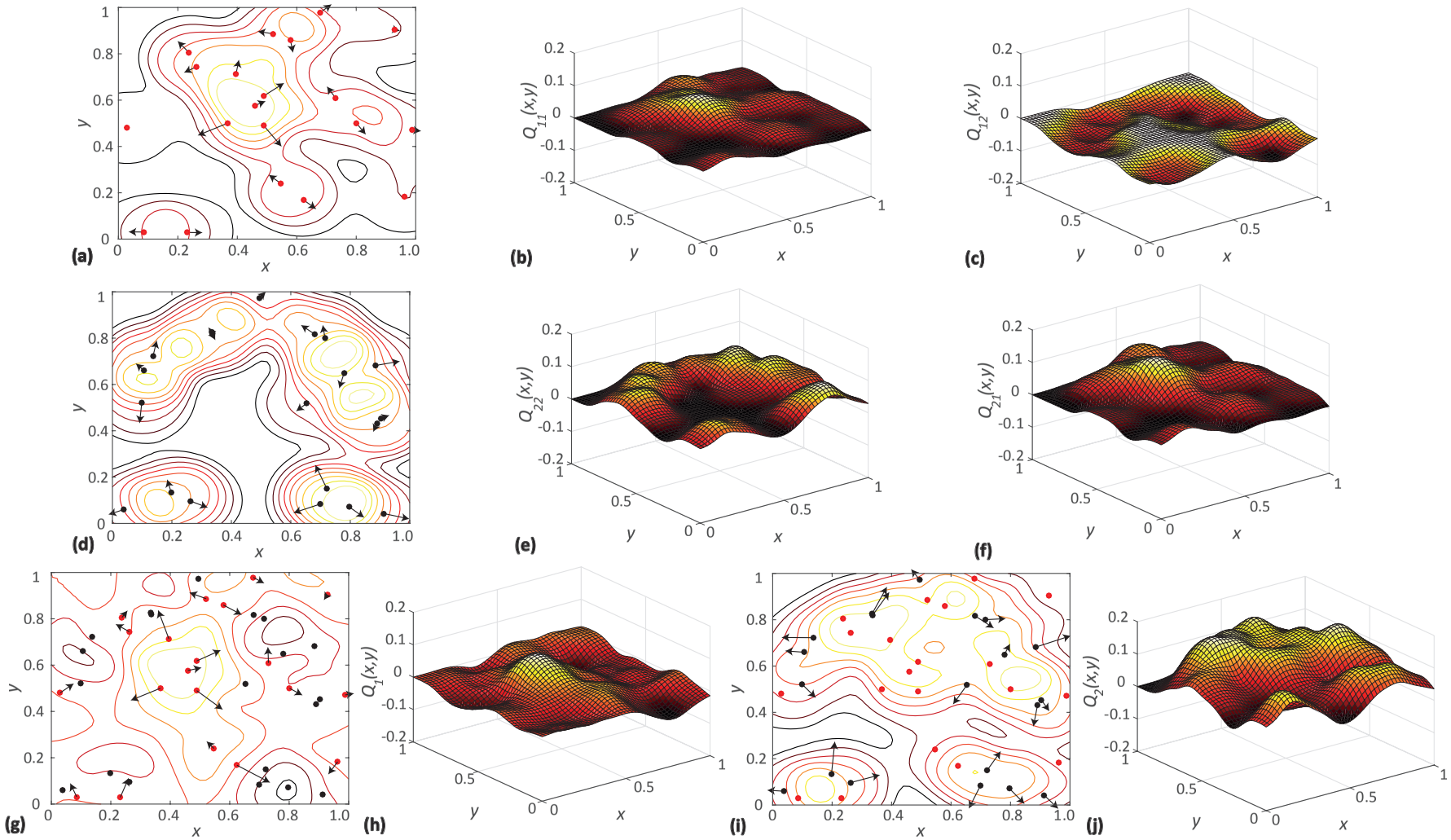

Figure 2. Visualisation of directional bias for a community consisting of two species. **a** shows the location of individuals of species 1. **d** shows the location of individuals of species 2. **g, i** shows the location of both species. In each subfigure, **a, d, g, i**, the locations of individuals are superimposed with the level curves of various components of the bias landscape. **b, c, e, f** shows the different components of the bias landscape: $Q_{11}(\mathbf{x})$; $Q_{12}(\mathbf{x})$; $Q_{21}(\mathbf{x})$; and $Q_{22}(\mathbf{x})$, respectively. **h,j** shows the net bias landscape of individuals of species 1 and 2, respectively. The bias vectors are shown with black arrows. The length of arrows indicate the strength of bias. Results in **a-b** correspond to interactions between individuals of species 1 only. Results in **d-e** show interactions between individuals of species 2 only. Results in **g-h** and **i-j** show the net interaction for both species. Parameter values are $\gamma_{11}^{(b)} = 0.1, \gamma_{12}^{(b)} = -0.1$, $\gamma_{21}^{(b)} = \gamma_{22}^{(b)} = 0.15$ and

Table 1. Table of model parameters and default values

Parameter	Symbol	Default value
Intrinsic movement rates	m_1, m_2	5
Bias interaction strengths	$\gamma_{11}, \gamma_{12}, \gamma_{21}, \gamma_{22}$	0, -0.2, 0.3, 0.3
Spatial extent of bias interactions	$\sigma_{11}, \sigma_{12}, \sigma_{21}, \sigma_{22}$	0.5
Mean movement distances	μ_1, μ_2	0.4
Standard deviation movement distances	$\sigma_1^{(s)}, \sigma_2^{(s)}$	0.1
Population size of species 1	N_1	200
Population size of species 2	N_2	200

5. Results

In this section, we explore how different features of the intraspecies and interspecies interactions influence the spatial structure of a two species community using the IBM and spatial moment models. First, we explore the time evolution of bias and spatial structure of the community by showing snapshots of the bias landscapes and PCFs at different times. Next, we examine the influence of variation in factors such as interaction strength, spatial extent of interaction and relative density of species, in determining the macroscale spatial patterns at a sufficiently large time that the system has reached a statistically stationary state. A summary of the key parameters used for these simulations is given in Table 1.

5.1. Evolution of bias and spatial structure

Here, we explore how the bias and spatial structure of a two species community evolve as individuals undergo movement events. To illustrate, we consider a sample community consisting of individuals from two distinct species with population sizes $N_1 = 30$ and $N_2 = 30$ and random initial placement of individuals. In this suite of simulations, we use a negative value for γ_{12} which means that individuals of species 1 are attracted to individuals of species 2. All the three remaining bias strength parameters are chosen to be positive, which corresponds to repulsion between conspecific individuals and repulsion of individuals of species 2 from individuals of species 1. These choices of bias strength parameters give rise to a chase-escape interaction. Results in Figure 3 show a series of snapshots of the location of individuals, bias landscapes of both the species and PCFs computed at $t = 0, 1, 20$, and 40, respectively, from the IBM.

In Figure 3(a)-(d) we see the evolution of bias vectors as the individuals start to

move. As time progresses, the locations of individuals changes due to the movement of individuals. That implies the local environment around individuals keeps changing and hence the neighbourhood contribution to the bias vector of an individual also varies. The evolution of bias landscapes $Q_1(\mathbf{x})$ and $Q_2(\mathbf{x})$ are shown in Figure 3(e)-(h) and Figure 3(i)-(l), respectively. The transition of the spatial structure of the community from the initial spatial Poisson process is explored by plotting the auto-correlation and cross-correlation PCFs $C_{11}(r), C_{22}(r)$ and $C_{12}(r)$, respectively as shown in Figure 3(m)-(p). Comparing the results at $t = 20$ and $t = 40$ suggests that we have an approximately steady spatial pattern established by $t = 20$. As time progresses, we observe the development of regular spatial pattern among subpopulations of species 1 and species 2 since $C_{11}(r) < 1$ and $C_{22}(r) < 1$ for small distances. The reason for the regular spatial structure is the intraspecies repulsion among individuals of both the species. Each individual of species 1 (species 2) tries to stay apart from other individuals of species 1 (species 2), hence lead to a regular spatial structure among individuals of species 1 (species 2). We also observe a less pronounced interspecies regular spatial pattern between individuals of species 1 and species 2. The attractive bias of species 1 to species 2 counteracts the repulsive bias of species 2 to species 1, reducing the extent of the interspecies regular spatial pattern.

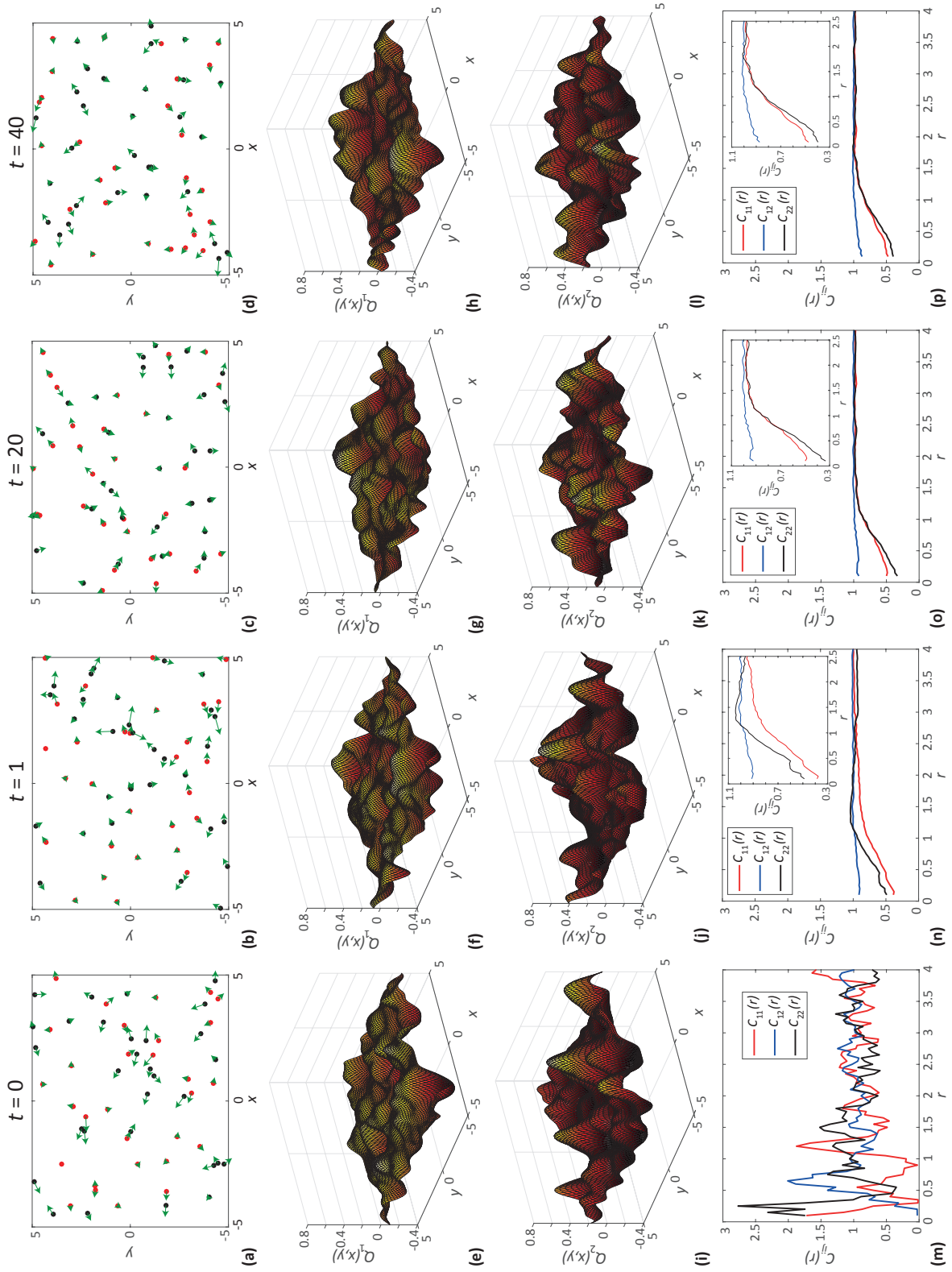

Figure 3. Results in **a-d** show the location of individuals of species 1 (red) and species 2 (black) along with the bias vectors at $t = 0, 1, 20$ and 40, respectively. The bias vectors are denoted by green arrows. Results in **e-h** show the bias landscape $Q_1(\mathbf{x})$ at $t = 0, 1, 20$ and 40, respectively. Results in **i-l** show the bias landscape $Q_2(\mathbf{x})$ at $t = 0, 1, 20$ and 40, respectively. Results in **m-p** show the PCFs $C_{11}(r)$, $C_{12}(r)$, $C_{22}(r)$ as a function of separation distance r at $t = 0, 1, 20$ and 40, respectively. The PCFs in **m** corresponds to the randomly

5.2. Effect of varying the interaction strength

Here, we perform a comprehensive investigation of how variations in bias interaction strength influence the development of spatial structure in the community. In our simulations, we consider a community composed of individuals from two distinct species with a random initial distribution with $N_1 = 200$ and $N_2 = 200$. Note that the random distribution of individuals means that there is no initial spatial structure. We systematically vary the interaction strengths γ_{12}, γ_{21}, and γ_{22} to explore the role of different intraspecies and interspecies interaction mechanism in determining the spatial pattern. For simplicity, in all simulations, we assume $\gamma_{11} = 0$ which means that species 1 has no intraspecific interactions. We compute the auto-correlation PCFs, $C_{11}(r)$ and $C_{22}(r)$, and cross-correlation PCF $C_{12}(r)$ along with metrics A_{11}, A_{12} and A_{22}, to quantify the resulting spatial patterns generated in the community. The results of the simulations are given in Figure 4. The three rows in Figure 4 show the simulation results of IBM along with the prediction of spatial moment dynamics for different values of γ_{12}, γ_{21}, and γ_{22}, respectively.

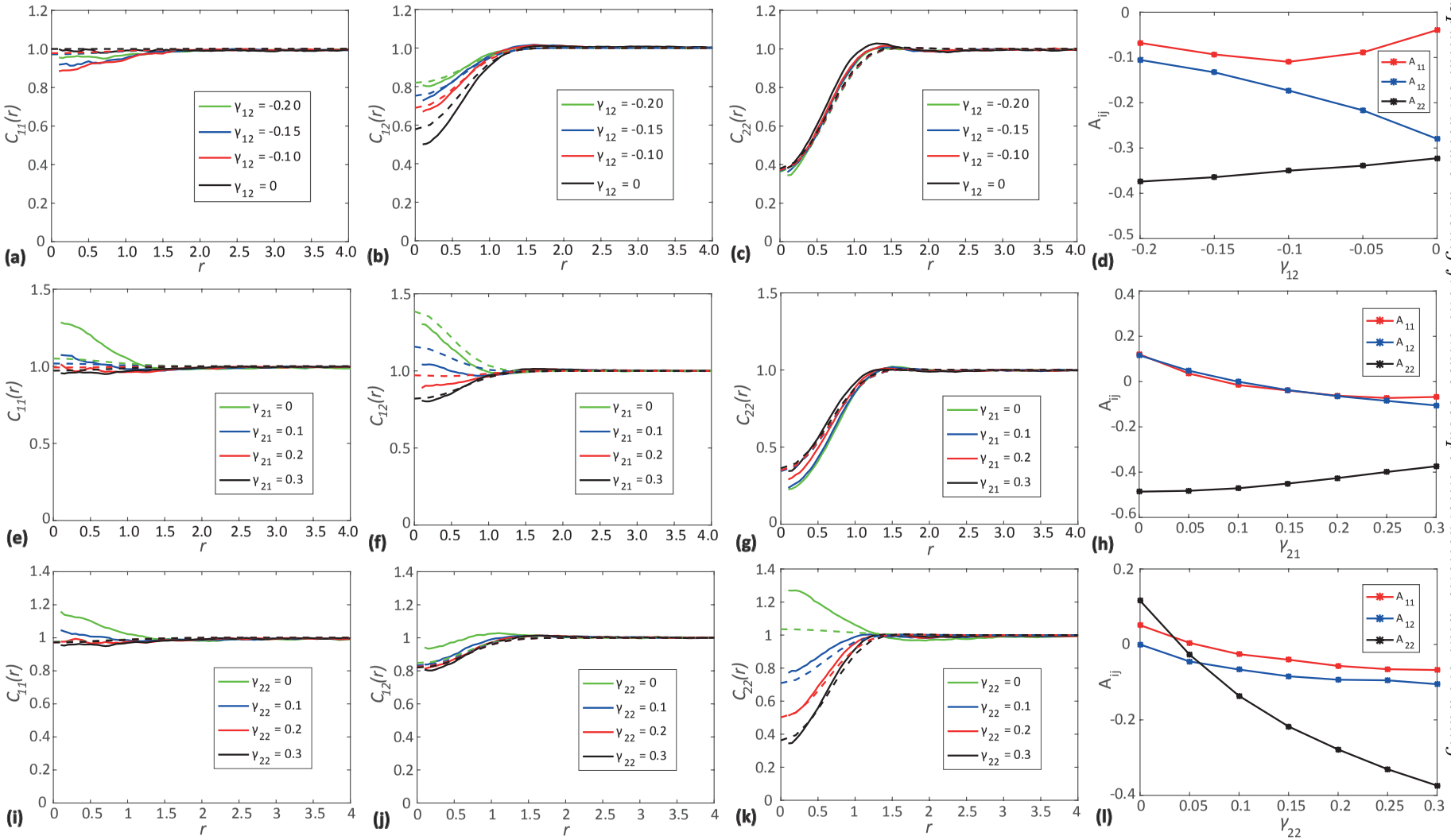

Figure 4. Effects of varying the interaction strength. **a-c** show the PCFs $C_{11}(r)$, $C_{12}(r)$, $C_{22}(r)$ as a function of separation distance for different choices of γ_{12}. **d** shows the metric as a function of γ_{12}. **e-g** show the PCFs $C_{11}(r)$, $C_{12}(r)$, $C_{22}(r)$ as a function of separation distance for different choices of γ_{21}. **h** shows A_{ij} as a function of γ_{21}. **i-k** show the PCFs $C_{11}(r)$, $C_{12}(r)$, $C_{22}(r)$ as a function of separation distance for different choices of γ_{22}. **l** shows A_{ij} as a function of γ_{22}. In subfigures showing PCFs as a function of r, solid curves show the averaged results from 1000 identically prepared realisations of the IBM, whereas dashed curves correspond to results from spatial moment dynamics model. In all results, PCFs and metrics are given at $t = 20$. Parameter values are $m_1 = m_2 = 5.0$, $\gamma_{11} = 0$, $\sigma_{11} = \sigma_{12} = \sigma_{21} = \sigma_{22} = 0.5$, $\mu_1^{(s)} = \mu_2^{(s)} = 0.4$, $\sigma_1^{(s)} = \sigma_2^{(s)} = 0.1$

Figure 4(a)-(d) shows the impact of varying γ_{12} that determine the contribution of individuals of species 2 to the bias vector associated with individuals of species 1. For these set of simulations, we use constant values of $\gamma_{21} = 0.3$ and $\gamma_{22} = 0.3$ representing repulsive interactions, so that we can focus on the influence of γ_{12}. When $\gamma_{12} = 0$, the auto-correlation PCF of species 1 is close to one, indicating the absence of intraspecies spatial structure among individuals of species 1. In the absence of neighbourhood contribution to the bias vector, the direction of movement becomes uniformly distributed. Hence no specific spatial structure is observed. In contrast, we see that $C_{12}(r)$ and $C_{22}(r)$ are less than 1 for small distances, suggesting an interspecies regular spatial pattern among individuals of species 1 and 2, as well as an intraspecies regular pattern among individuals of species 2. When $\gamma_{12} = 0$, there is no opposing effect to the repulsion of species 2 to species 1. Hence, both species will be located away from each other forming a regular pattern. Similarly, individuals of species 2 stay away from other individuals of the same species due to the intraspecies repulsion. As we introduce an attractive bias for individuals of species 1 towards species 2, by making γ_{12} negative, an intraspecies regular spatial structure emerges among individuals of species 1. This is due to the fact that, individuals of species 1 tend to move towards individuals of species 2 and the regular arrangement of species 2 forces species 1 to occupy spaces around species 2. The interspecies regular spatial pattern becomes less pronounced as γ_{12} is made negative. As γ_{12} becomes more negative, the enhanced attractive bias starts to counteract the interspecies repulsive bias formed due to positive γ_{21}. This result in a reduction of segregation between individuals of species 1 and 2. These observations are also confirmed by the metric A_{12}. As γ_{12} is made more negative, A_{12} gets closer to zero.

Results in Figure 4(e)-(h) show how varying the bias strength γ_{21} which specifies the nature of the contribution of individuals of species 1 on individuals of species 2. Here, we fix $\gamma_{12} = -0.2$, and $\gamma_{22} = 0.3$, representing attraction of species 1 to 2 and repulsive interactions among individuals of species 2. When $\gamma_{21} = 0$, we see that $C_{11}(r)$ and $C_{12}(r)$ greater than 1 for small distances, suggesting an intraspecies clustering among individuals of species 1 and interspecies clustering between individuals of species 1 and 2. The metrics A_{11} and A_{12} are positive for $\gamma_{21} = 0$, also confirms this observation. In the absence of repulsion from species 2, the attractive bias of individuals of species 1 to species 2 act solely to move individuals of species 1 towards species 2. This results in accumulation of individuals of species 1 around individuals of species 2, forming clusters. On the other hand, repulsion between individuals of species 2 results in an intraspecies regular spatial pattern among individuals of species 2. With the increase in γ_{21}, the clustering weakens and for a sufficiently large choice of gamma $\gamma_{21} = 0.3$, the spatial structure changes to the regular spatial pattern. When γ_{21} is large enough, the repulsive bias of species 2 towards species 1 overcomes the attractive bias of species 1 to species 2. This dominant repulsive bias results in overall segregation of individuals of species 1 and 2, developing a regular spatial pattern. Another interesting result is that the intraspecies segregation between individuals of species 2 weakens as we increase γ_{21}. In spite of the repulsion between individuals of species 2, the enhanced repulsion of species

2 from species 1 result in individuals of species 2 coming closer to each other.

Results in Figure 4(i)-(l) show how varying the bias strength γ_{22} that specify the nature of the intraspecies contribution of individuals of species 2. Now we fix $\gamma_{12} = -0.2$, and $\gamma_{21} = 0.3$, representing attraction of species 1 to 2 and repulsion of species 2 to 1. We observe a strong regular spatial pattern emerges in the subpopulation of species 2. This can be attributed to the increased repulsive bias between individuals of species 2 as we increase the interaction strength γ_{22}. Finally, we observe that the accuracy of the spatial moment prediction increases with the bias interaction strength.

5.3. Effect of varying the spatial extent of interaction

Here, we investigate how varying the range of interactions impact the formation of spatial structure. The spatial extent of interaction, σ_{ij} determines the range over which the interactions between individuals are significant. A small choice of σ_{ij} leads to short-range interactions, whereas a large σ_{ij} corresponds to long-range interactions between individuals. Again, we consider a community consisting of individuals of two different species with $N_1 = 200$ and $N_2 = 200$, respectively, with a random initial distribution of individuals. We systematically vary the spatial extent of interaction σ_{12} and σ_{21} corresponding to the interspecies interaction of species 1 and 2, as well as σ_{22} corresponding to the intraspecies interaction of species 2. As before we set $\gamma_{11} = 0$ which means that intraspecific interactions in species 1 are switched off.

Results in Figure 5(a)-(d) show the effects of varying the spatial extent of interaction, σ_{12} that corresponds to the interaction kernel specifying contribution of individuals of species 2 on the bias vector of individuals of species 1. We observe that the cross-correlation PCF $C_{12}(r)$ becomes close to unity, suggesting a shift from the interspecies regular spatial pattern between individuals of species 1 and 2, as we increase σ_{12}. This is also confirmed by the increase of A_{12} with the increase in σ_{12}. This behaviour arises because of the fact that, as we increase the spatial extent of interactions the distance over which individuals of species 2 influence the bias vector of individuals of species 1 increases. This results in an enhanced attractive bias that destroys the regular spatial pattern.

Figure 5(e)-(h) shows the impact of varying the spatial extent of interaction, $\sigma_{21}(\boldsymbol{\xi})$, that corresponds to the interaction kernel specifying the contribution of individuals of species 1 on the bias vector of individuals of species 2. We observe a small scale intraspecies clustering among individuals of species 1 and interspecies clustering between individuals of species 1 and species 2 for small values of σ_{21}. Also, a regular spatial pattern emerges between individuals of species 2. As σ_{21} increases, the clustering becomes weak and changes to a regular spatial structure for a sufficiently large spatial extent of interaction. This trend is confirmed by A_{11} and A_{12}. Both of these metrics changes from a positive value at $\sigma_{21} = 0.25$ to negative values as we increase σ_{21}. As we increase σ_{21}, individuals of species 1 experience strong repulsion due to the added effect of more distant individuals of species 2. This results in the segregation of individuals of

species 1 and species 2. The intraspecies regular spatial pattern of individuals of species 2 becomes less pronounced with the increase in the spatial extent of interaction

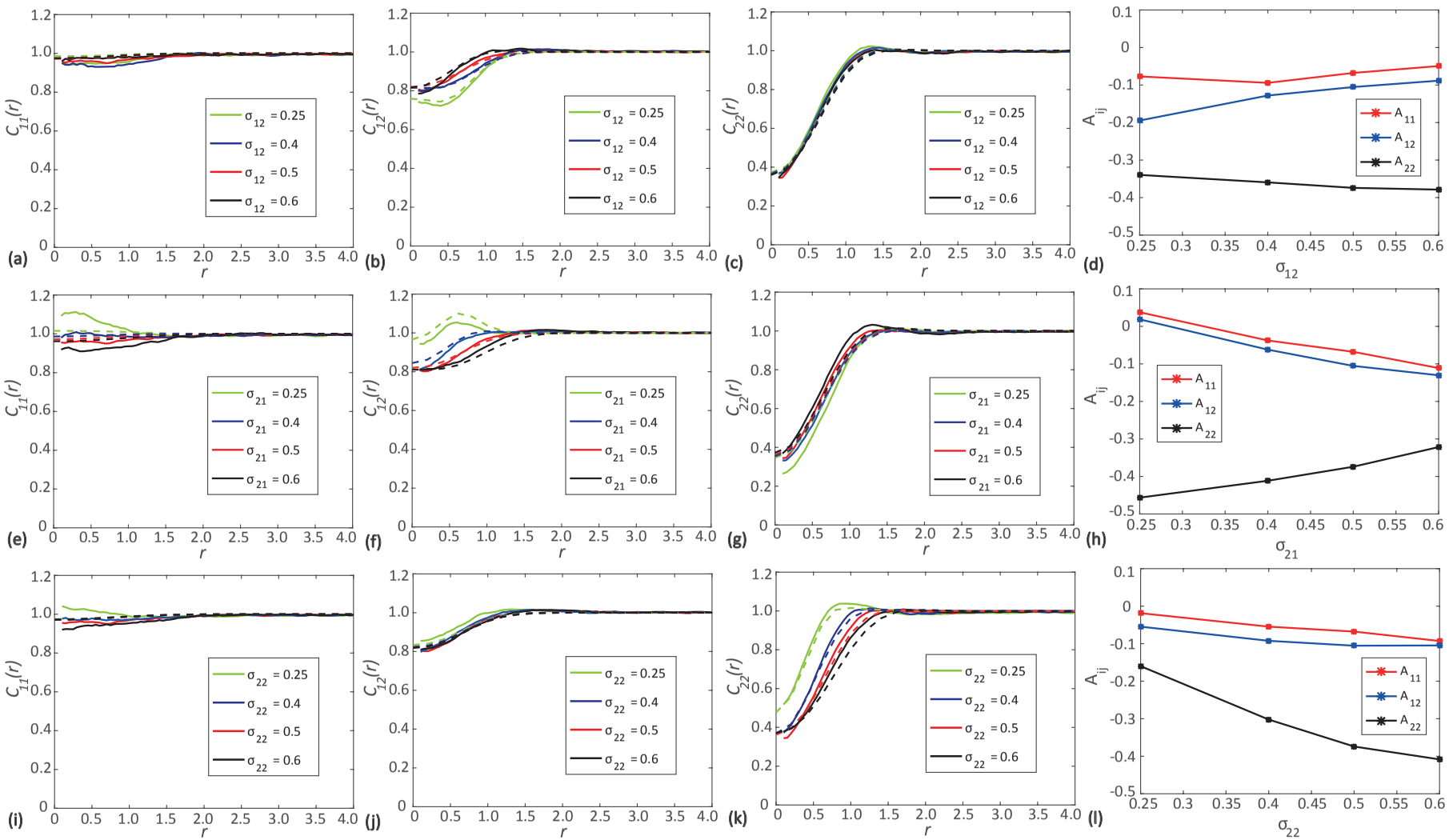

Figure 5. Effects of varying the spatial extent of interaction. **a-c** show the PCFs $C_{11}(r)$, $C_{12}(r)$, $C_{22}(r)$ as a function of separation distance for different choices of σ_{12}. **d** shows A_{ij} as a function of σ_{12}. **e-g** show the PCFs $C_{11}(r)$, $C_{12}(r)$, $C_{22}(r)$ as a function of separation distance for different choices of σ_{21}. **h** shows A_{ij} as a function of σ_{21}. **i-k** show the PCFs $C_{11}(r)$, $C_{12}(r)$, $C_{22}(r)$ as a function of separation distance for different choices of σ_{22}. **l** shows the metric as a function of σ_{22}. In subfigures showing PCFs as a function of r, solid curves show the averaged results from 1000 identically prepared realisations of the IBM, whereas dashed curves correspond to results from spatial moment dynamics model. In all results, PCFs and metrics are given at $t = 20$. Parameter values are $m_1 = m_2 = 5.0$, $\gamma_{11} = 0, \gamma_{12} = -0.2, \gamma_{21} = \gamma_{22} = 0.3$, $\mu_1^{(s)} = \mu_2^{(s)} = 0.4$, $\sigma_1^{(s)} = \sigma_2^{(s)} = 0.1$.

Finally, we vary the spatial extent of interaction, σ_{22}, that corresponds to the interaction kernel specifying the intraspecies contribution of individuals of species 2, as shown in Figure 5(i)-(l). With respect to increase in σ_{22}, we see the $C_{22}(r)$ diverges from unity suggesting a stronger spatial regular pattern among individuals of species 2. The metric A_{22} decreases with σ_{22} confirming the formation of more pronounced regular spatial pattern among individuals of species 2. The increase in σ_{22} enables an individual of species 2 to influence more distant individuals of species 2, enhancing the regular structure. Our results also show that the spatial moment model gives a more accurate approximation of the IBM for small σ_{ij} values.

5.4. Effect of varying the relative density of species

We now explore how varying the relative density of individuals of species 1 and 2, $Z_{1,1}/Z_{1,2}$, impacts the spatial configuration of the community. We consider a community composed of different density ratios, $Z_{1,1}/Z_{1,2} = 1/7, 3/5, 1$ and 7, respectively. To vary the relative density of species 1, the total number of individuals in the community is fixed at $N_1 + N_2 = 400$ and the population size of species 1 is varied as $N_1 = 50, 150, 200$ and 350, respectively. In all cases, we consider a randomly distributed initial arrangement of individuals. We investigate the behaviour of spatial pattern in the community by plotting the PCFs and metric as shown in Figure 6.

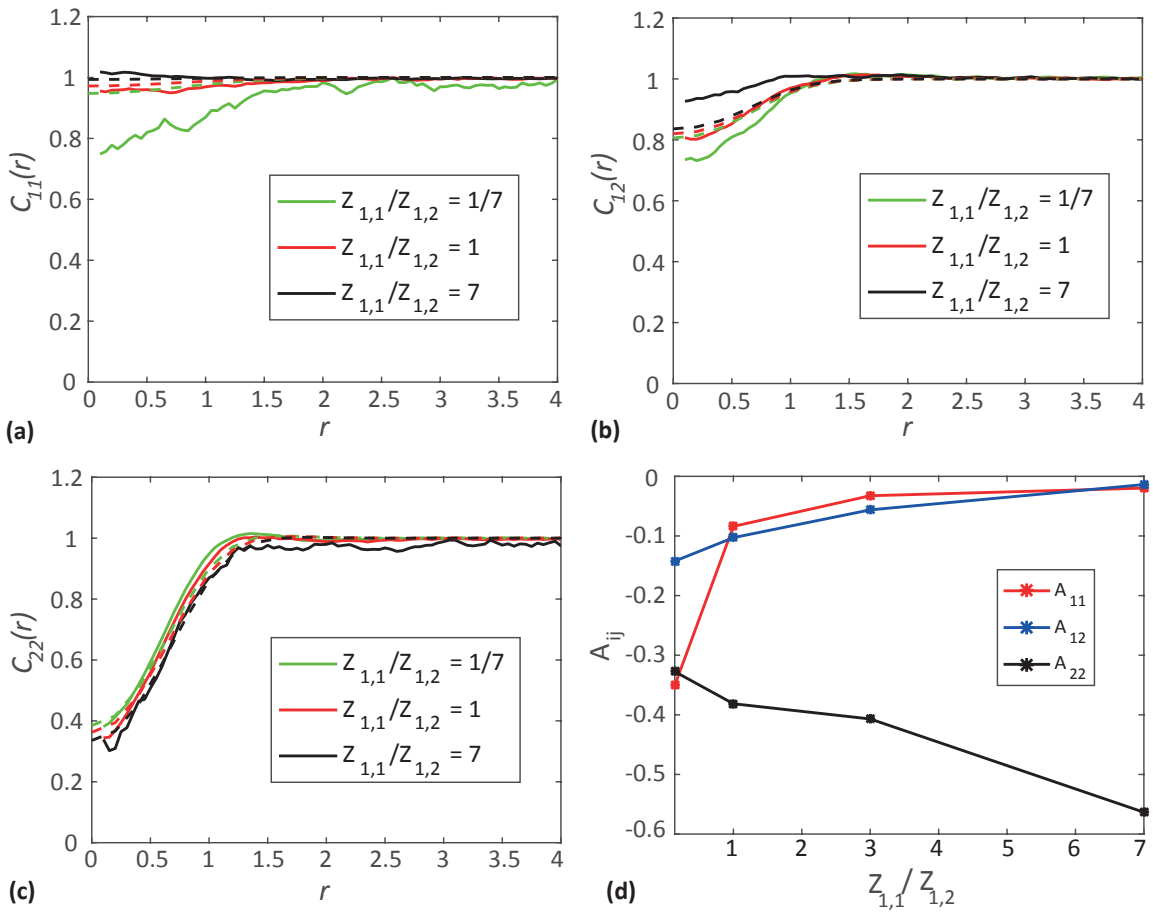

Figure 6. Effects of varying the relative density of species. **a** shows the auto-correlation PCF of species 1 as a function of separation distance. **b** shows the cross-correlation PCF as a function of separation distance. **c** shows the auto-correlation PCF of species 2 as a function of separation distance. **d** shows A_{ij} as a function of relative densities of species. In (**a**)-(**c**) solid curves show the averaged results from 1000 identically prepared realisations of the IBM, whereas dashed curves correspond to results from spatial moment dynamics model. In all results, PCFs and metrics are given at $t = 20$. Parameter values are $m_1 = m_2 = 5.0$, $\gamma_{11} = 0, \gamma_{12} = -0.2, \gamma_{21} = \gamma_{22} = 0.3$, $\sigma_{11} = \sigma_{12} = \sigma_{21} = \sigma_{22} = 0.5$, $\mu_1^{(s)} = \mu_2^{(s)} = 0.4$, $\sigma_1^{(s)} = \sigma_2^{(s)} = 0.1$.

As we increase the relative density of species 1, the auto-correlation PCF of individuals of species 1 becomes close to one and metric A_{11} gets closer to zero. These observations suggest that the intraspecies regular spatial structure among individuals of species 1 weakens as relative density of species 1 increases. At a low relative density of species 1, individuals of species 1 move close to a neighbouring individual of species 2 due to the choice of negative γ_{12}. Since the density of species 2 is much higher compared to species 1, individuals of species 1 could be placed far apart from other individuals of species 1, creating an intraspecies regular spatial structure. In contrast, at a high relative

density of species 1, more individuals of species 1 tend to move towards a particular individual of species 2, resulting in an accumulation of individuals of species 1 at short distances leading to a less regular spatial structure.

Another observation from the results in Figure 6 is that the auto-correlation PCF of species 2 diverges from unity indicating a stronger intraspecies regular spatial pattern emerges among individuals of species 2. The metric A_{22} becomes more negative with the increase of relative density of species 1 also confirms this behaviour. This is a counterintuitive result since we are seeing stronger regular structure in species 2 as its population size decreases. This is an indirect effect of interactions of species 2 with species 1. At a high relative density of species 1, each individual of species 2 will be surrounded by many individuals of species 1. The repulsive bias of species 2 to species 1 forbids possible movement of any individuals of species 2, towards other individuals of species 2, that are surrounded by individuals of species 1. This results in a segregation between individuals of species 2. Hence we see an intraspecies regular structure of species 2 at high relative density of species 1.

The cross-correlation PCF in Figure 6 becomes close to one and A_{12} approaches zero as we increase the relative density of species 1. That implies the interspecies regular spatial pattern weakens as the relative density of species 1 is increased. As we increase the relative density of species 1, the effects of interaction driven by individuals of species 1 dominate the contribution of individuals of species 2. Hence, the attraction of species 1 to species 2 out-compete the repulsive bias of species 2 to species 1, to create a less regular spatial pattern. We also observe that the best match between spatial moment prediction and IBM is when the relative density is equal to one.

We conclude by presenting another set of results, as shown in Figure 7, to emphasise that the impact of variation in relative density is strongly dependent on the choice of interaction strengths. To illustrate this point, we consider a scenario with same parameter choice and initial placement of individuals as in Figure 6, except for that we vary interaction strength γ_{12}. In contrast to the choice of a negative γ_{12} that corresponds to an attractive bias in Figure 6, for this suite of simulations, we choose a positive γ_{12} that corresponds to the case where species 1 repels species 2. In contrast to to the results in Figure 6(a), we observe a strong clustering of species 1 when the relative density of species 1 is low. At low relative densities of species 1, the presence of more number of individuals of species 2 creates a strong repulsion to fewer individuals of species 1. Choosing $\gamma_{12} = 0.3$ forces individuals of species 1 to move away from the neighbourhood of species 2. Since there is no interaction between individuals of species 1, both these factors act together to drive individuals of species 1 to form clusters. As we increase the relative density of species 1, the clustering weakens and leads to a random spatial structure. The metric A_{11} reduces from 1.5 at $Z_{1,1}/Z_{1,2} = 1/7$ and approaches zero as

we increase the relative density of species 1, also confirms this observation.

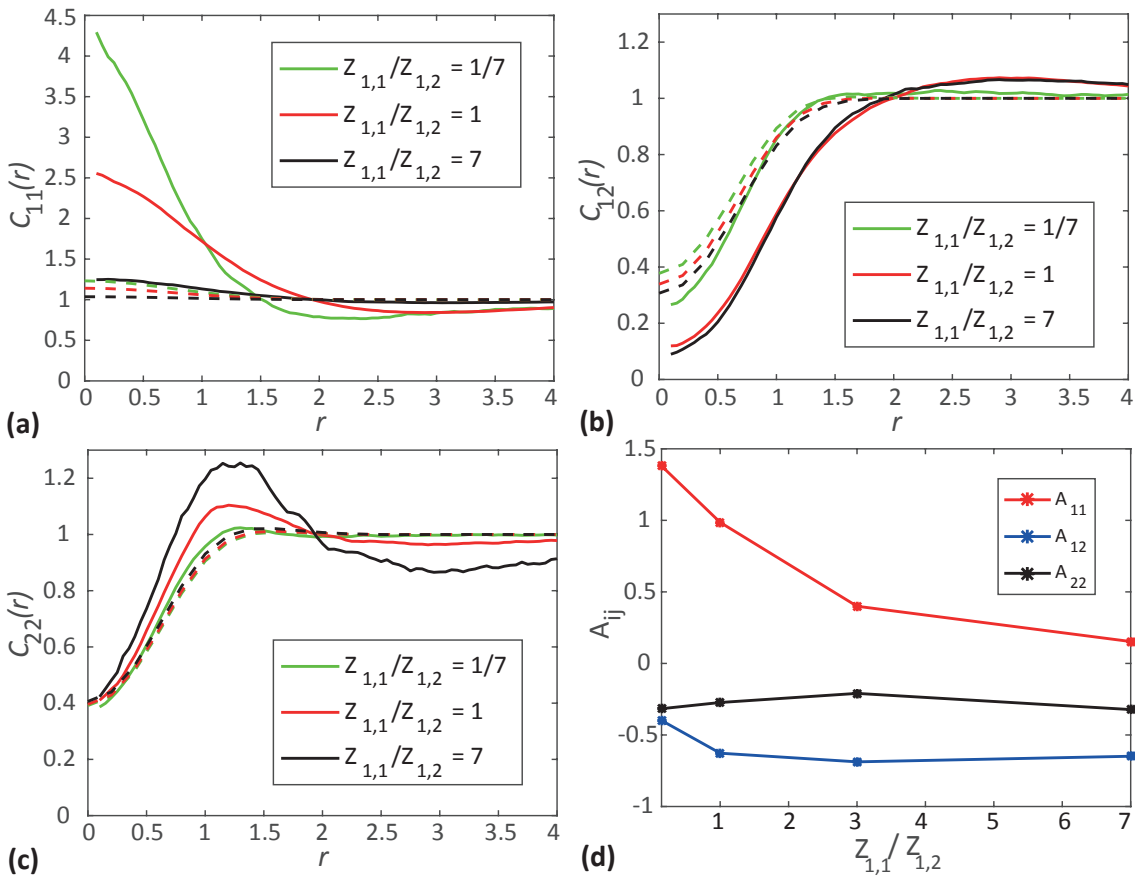

Figure 7. Effects of varying the relative density of species. **a** shows the auto-correlation PCF of species 1 as a function of separation distance. **b** shows the cross-correlation PCF as a function of separation distance. **c** shows the auto-correlation PCF of species 2 as a function of separation distance. **d** shows A_{ij} as a function of relative densities of species. In (**a**)-(**c**) solid curves show the averaged results from 1000 identically prepared realisations of the IBM, whereas dashed curves correspond to results from spatial moment dynamics model. In all results, PCFs and metrics are given at $t = 20$. Parameter values are $m_1 = m_2 = 5.0$, $\gamma_{11} = 0, \gamma_{12} = \gamma_{21} = \gamma_{22} = 0.3$, $\sigma_{11} = \sigma_{12} = \sigma_{21} = \sigma_{22} = 0.5$, $\mu_1^{(s)} = \mu_2^{(s)} = 0.4$, $\sigma_1^{(s)} = \sigma_2^{(s)} = 0.1$.

At low relative densities of species 1 we observe an intraspecies regular spatial pattern of species 2 due to the repulsive interaction between individuals of species 2. As we increase the relative density of species 1, we observe a peak in $C_{22}(r)$ at approximately $r = 1.25$. This peak corresponds to an extreme case of regular spatial pattern where almost all individuals of species 2 are separated by approximately the same distance. The more pronounced regular pattern arises due to the combined effect of the enhanced repulsion of species 1 to species 2 due to the increase in the number of individuals of

species 1 compared to species 2 and the repulsive intraspecies interaction of species 2. Overall, we summarise that the interspecies regular spatial structure between species 1 and species 2 becomes more pronounced as the relative density of species 1 increases.

6. Conclusions

In this work, we present a generalised IBM that describes the movement of individuals in a community consisting of multiple species with various interaction among individuals. This modelling framework allows us to capture different features of the individual-level motility mechanisms such as neighbour dependent directional bias arising as a consequence of the interactions among individuals. We explore a range of complex spatial structure patterns arising from the combined impacts of various intraspecies interactions and interspecies interactions in a stereotypical community consisting of two distinct species. To provide additional insight into the IBM, we derive a macroscale deterministic approximation of the stochastic IBM using spatial moment dynamics. The spatial moment dynamics approach provides us with a mathematically tractable method to characterise the IBM. Our model accommodates numerous scenarios involving different types of attractive or repulsive bias arising between individuals of different species. We provide an extensive analysis of different features of the intraspecies and interspecies interaction by varying the interaction strength, the spatial extent of interaction and relative densities of individuals of both the species.

Our results show that across a range of parameter values the spatial moment dynamics model provides a reasonable approximation to the IBM. The combined IBM and spatial moment dynamics analysis reveal the macroscale spatial patterns, such as intraspecies and interspecies clustering and regular spatial patterns, that arise as a result of the movement of individuals under the influence of neighbour-dependent directional bias. Our results include several interesting and possibly counter-intuitive results such as the increase in density of species 1 relative to species 2 results in weakening of regular pattern between individuals of species 1 and enhancement of regular pattern among individuals of species 2, for the parameter values considered.

In addition to pointing out how our IBM enables us to encode various types of intraspecies and interspecies interactions, including various strengths of chase-escape interactions, perhaps the most striking feature of our analysis is that we find the formation of, at times, strong spatial structure that is driven purely by motility. This is very interesting because most spatial moment models and analysis have their origin in plant ecology where birth and death are the key mechanisms and motility is irrelevant (Bolker and Pacala 1997; Bolker and Pacala 1999; Law and Dieckmann 2000; Law et al. 2003). More recent spatial moment models have been developed to mimic cell biology experiments where simultaneous movement and proliferation are important, and these previous studies attribute the formation of spatial structure to the combined effects of motility and proliferation (Binny et al. 2016b; Browning et al. 2017). As far as we

are aware, this is the first study to apply spatial moment analysis to a conservative population, composed of multiple distinct communities, without birth or death events. This enables us to focus on how motility alone drives significant spatial patterning, and we find that this is particularly relevant when we consider asymmetric interactions between those distinct communities within the population.

An interesting extension of the model presented here would be to include interactions which affect the proliferation and mortality of individuals, such as predator-prey interactions or intra and interspecific competition. The population dynamics resulting from such interactions will depend on the types spatial structure examined in this work. Another extension would be to consider spatial processes such as moving fronts that are relevant to many biological processes including malignant invasion and developmental morphogenesis (Johnston et al. 2017; Smith and Yates 2018). We leave these extensions for future work.

Appendix A. Numerical simulation of the individual based model

We use the Gillespie algorithm (Gillespie 1977) to simulate the IBM. In all cases we consider a community composed of I distinct species composed of N_i individuals distributed across a square domain of size $L \times L$. All simulations are initialised by distributing all individuals according to a spatial Poisson process. The intrinsic movement rate of an individual from species i is m_i, and the net movement rate of the community is,

$$\lambda = \sum_{i=1}^{I} m_i \, N_i. \tag{A.1}$$

The time interval between successive movement events is exponentially distributed with mean $1/\lambda$. When a motility event is to take place, a individual is chosen to move at random. The chosen individual moves a displacement $\boldsymbol{\xi}$ specified by the movement displacement PDF, $\mu_i(\boldsymbol{\xi}; \widehat{\mathbf{B}}_n)$.

We use spatial moments to characterise the spatial structure in the population. The first spatial moment of individuals of species i is $Z_{1,i} = N_i/L^2$. Note that the first moment is always constant. We analyse the spatial structure of the community using the second spatial moment expressed as a PCF. In our model we have two distinct types of PCFs namely: (i) the auto-correlation PCF corresponds to individuals of same species, $C_{ii}(r)$, and (ii) the cross-correlation PCF corresponds to individuals of different species $C_{ij}(r)$. To compute the auto-correlation PCF for species i, we choose a reference individual for species i, located at $\mathbf{x}_n$ and compute all distances, $r = |\mathbf{x}_r - \mathbf{x}_n|$ from all other individuals of species i. We repeat this procedure until each of the remaining $N_i - 1$ individuals in species i act as a reference individual. The PCF is constructed by counting all the distances that fall into the interval $[r - \delta r/2, r + \delta r/2]$. Normalising the bin count by a factor of $N_i\,(N_i - 1)(2\pi r \delta r)/L^2$ gives C_{ii} such that $C_{ii}(r) = 1$ corresponds to a complete absence of spatial structure. Similarly, we compute the cross-correlation PCF,

$C_{ij}(r)$, by enumerating the distance between all possible pairs consisting of individuals of species i and j, and then normalising these counts.

Appendix B. Numerical methods for spatial moment dynamics

The numerical solution for the dynamical equation of the second spatial moment, Equation 7 is computed using the forward Euler method. This scheme involves a spatial discretisation of the displacement, $\boldsymbol{\xi} = (\xi_x, \xi_y)$, using a square grid with constant spacing, $\Delta\xi$, over the domain $\{-\xi_{\max} \leq \xi_x, \xi_y \leq \xi_{\max}\}$. Her, $\xi_{\max}$ is chosen to be sufficiently large such that the second spatial moments are given by a mean field condition at the domain boundaries, giving, $Z_{2,ij}(\boldsymbol{\xi}, t) \approx Z_{1,i} \times Z_{1,j}$. The integral terms in Equation 5 and Equation 7 are approximated using the trapezoid rule. To compute these integrals, we need to evaluate $Z_{2,ij}(\boldsymbol{\xi} \pm \boldsymbol{\xi}')$ for different combinations of $\boldsymbol{\xi}$ and $\boldsymbol{\xi}'$. Some of these combinations require values of $Z_{2,ij}(\boldsymbol{\xi} \pm \boldsymbol{\xi}')$ that lie beyond the computational domain. Whenever this scenario arises, we approximate those terms with the values of $Z_{2,ij}(\boldsymbol{\xi}, t)$ at the boundary, $Z_{2,ij}((\xi_{\max}, \xi_{\max}), t)$.

The initial condition used for solving the spatial moment dynamics is $Z_{2,ij}(\boldsymbol{\xi}, 0) = Z_{1,i} \times Z_{1,j}$. We use a constant grid spacing $\Delta\xi = 0.2$ and time step $\mathrm{d}t = 0.1$ in all our results. Additional results (not shown) confirms that this choice of spatial and temporal discretisation is sufficient to produce grid-independent results. We compare the numerical solution of the spatial moment dynamics model with the IBM simulation results by computing the auto-correlation PCF and cross-correlation PCF $Z_{2,ii}(\boldsymbol{\xi}, t)/Z_{1,i}^2$ and $Z_{2,ij}(\boldsymbol{\xi}, t)/(Z_{1,i}(t)Z_{1,j}(t))$, respectively.

Appendix C. Moment closure schemes

Here, we compare the accuracy of four popular moment closure schemes. The closure schemes considered include the power-1 closure, symmetric and asymmetric power-2 closures and Kirkwood superposition approximation (KSA) (Murrell et al. 2004; Raghib et al. 2011).

The power-1 closure is given by,

$$\begin{aligned} Z_{3,ijk}(\boldsymbol{\xi}, \boldsymbol{\xi}', t) = {} & Z_{1,i}\, Z_{2,jk}(\boldsymbol{\xi}' - \boldsymbol{\xi}, t) + Z_{1,j}\, Z_{2,ik}(\boldsymbol{\xi}', t) \\ & + Z_{1,k}\, Z_{2,ij}(\boldsymbol{\xi}, t) - 2Z_{1,i}\, Z_{1,j}\, Z_{1,k}. \end{aligned} \tag{C.1}$$

The power-2 closure is given by,

$$\begin{aligned} Z_{3,ijk}(\boldsymbol{\xi}, \boldsymbol{\xi}', t) = {} & \frac{1}{\alpha + \gamma}\Big[\alpha \frac{Z_{2,ij}(\boldsymbol{\xi}, t)\, Z_{2,ik}(\boldsymbol{\xi}', t)}{Z_{1,i}} + \beta \frac{Z_{2,ij}(\boldsymbol{\xi}, t)\, Z_{2,jk}(\boldsymbol{\xi}' - \boldsymbol{\xi}, t)}{Z_{1,j}} \\ & + \gamma \frac{Z_{2,ik}(\boldsymbol{\xi}', t)\, Z_{2,jk}(\boldsymbol{\xi}' - \boldsymbol{\xi}, t)}{Z_{1,k}} - \beta Z_{1,i} Z_{1,j} Z_{1,k}\Big]. \end{aligned} \tag{C.2}$$

For the symmetric power-2 closure, we choose $\alpha = \beta = \gamma = 1$, and for the asymmetric power-2 closure, we use $\alpha = 4, \beta = 1$, and $\gamma = 1$ (Law et al. 2003).

The Kirkwood superposition approximation is given by,

$$Z_{3,ijk}(\boldsymbol{\xi}, \boldsymbol{\xi}', t) = \frac{Z_{2,ij}(\boldsymbol{\xi}, t)\, Z_{2,ik}(\boldsymbol{\xi}', t)\, Z_{2,jk}(\boldsymbol{\xi}' - \boldsymbol{\xi}, t)}{Z_{1,i}\, Z_{1,j}\, Z_{1,k}}. \tag{C.3}$$

We compute PCFs using these different closure schemes for a community consisting of two species with $N_1 = N_2 = 100$ and compare with the averaged results of IBM simulation. Again, in these simulations, we consider a randomly distributed initial arrangement of individuals. Results in Figure C1 compare the auto-correlation PCFs, $C_{11}(r)$ and $C_{22}(r)$, and the cross-correlation PCF, $C_{12}(r)$, for each of the closure schemes with results from the IBM simulation. Overall, when we consider all three PFCs, we see that the power-2 asymmetric closure provides the best match with the prediction of the IBM simulation for the parameters considered in Figure C1. Our approach in this work is not to promote one particular closure approximation over another closure approximation. Instead, we present a general spatial moment framework that can be implemented with a range of closure assumptions should one particular closure approximation be preferred to another.

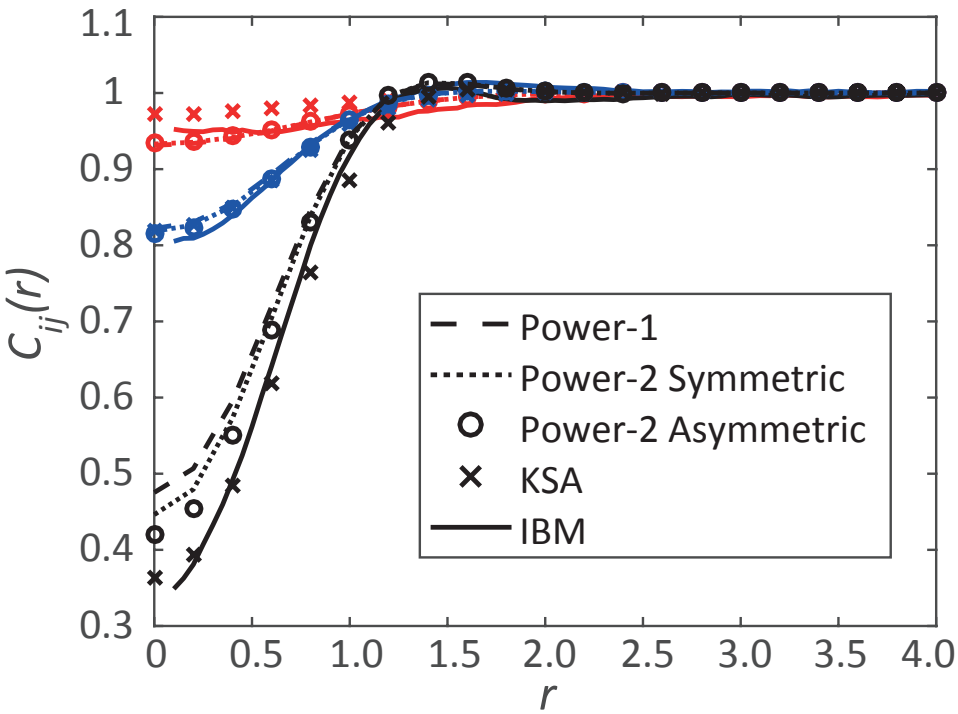

Figure C1. Comparison of spatial moment closure approximation schemes. The curves in red, blue and black correspond to $C_{11}(r), C_{12}(r)$ and $C_{22}(r)$, respectively. In all results, PCFs are given at $t = 20$. All PCFs from IBM correspond to averaged data of 1000 identically prepared realisations. Parameter values are $m_1 = m_2 = 5.0$, $\gamma_{11} = 0, \gamma_{12} = -0.2, \gamma_{21} = \gamma_{22} = 0.3$, $\sigma_{11} = \sigma_{12} = \sigma_{21} = \sigma_{22} = 0.5$, $\mu_1^{(s)} = \mu_2^{(s)} = 0.4$, $\sigma_1^{(s)} = \sigma_2^{(s)} = 0.1$.

References

Bajec I L and Heppner F H 2009 Organised flight in birds *Anim. Behav.* **78** 777–89

Barraquand F and Murrell D J 2013 Scaling up predator-prey dynamics using spatial moment equations *Methods Ecol. Evol.* **4** 276–89

Binny R N, Plank M J and James A 2015 Spatial moment dynamics for collective cell movement incorporating a neighbour-dependent directional bias *J. R. Soc. Interface* **12** 20150228

Binny R N, Haridas P, James A, Law R, Simpson M J and Plank M J 2016a Spatial structure arising from neighbour-dependent bias in collective cell movement *PeerJ* **4** e1689

Binny R N, James A and Plank M J 2016b Collective cell behaviour with neighbour-dependent proliferation, death and directional bias *Bull. Math. Biol.* **8** 2277–01

Bolker B M and Pacala S W 1997 Using moment equations to understand stochastically driven spatial pattern formation in ecological systems *Theor. Popul. Biol.* **52** 179–97

Bolker B M and Pacala S W 1999 Spatial moment equations for plant competition: understanding spatial strategies and the advantages of short dispersal *Am. Nat.* **153** 575–02

Charteris N and Khain E 2014 Modeling chemotaxis of adhesive cells: stochastic lattice approach and continuum description *New J. Phys.* **16** 025002

Dini S, Binder B J and Green J E F 2018 Understanding interactions between populations: Individual based modelling and quantification using pair correlation functions *J. Theor. Biol.* **439** 50–64

Dyson L, Maini P K and Baker R E 2012 Macroscopic limits of individual-based models for motile cell populations with volume exclusion *Phys. Rev. E* **86** 031903

Frasca M and Sharkey K J 2016 Discrete-time moment closure models for epidemic spreading in populations of interacting individuals *J. Theor. Biol.* **399** 13–21

Gavagnin E and Yates C A 2018 *Handbook of Statistics: Integrated Population Biology and Modelling* (Elsevier) 37–91

Gillespie D T 1977 Exact stochastic simulation of coupled chemical reactions *J. Phys. Chem.* **81** 2340–61

Green J E F, Waters S L, Whiteley J P, Edelstein-Keshet L, Shakesheff K M and Byrne H M 2010 Non-local models for the formation of hepatocyte-stellate cell aggregates *J. Theor. Biol.* **267** 106–20

Haridas P, Penington C J, McGovern J A, McElwain D L S and Simpson M J 2017a Quantifying rates of cell migration and cell proliferation in co-culture barrier assays reveals how skin and melanoma cells interact during melanoma spreading and invasion *J. Theor. Biol.* **423** 13–25

Haridas P, McGovern J A, McElwain D L S and Simpson M J 2017b Quantitative comparison of the spreading and invasion of radial growth phase and metastatic melanoma cells in a three-dimensional human skin equivalent model *PeerJ* **5** e3754

Inaba M, Yamanaka H and Kondo S 2012 Pigment pattern formation by contact-dependent

depolarization *Science* **335** 677

Janeway C, Travers P, Walport M and Shlomchik M 2005 *Immunobiology: The Immune System in Health and Disease* 6th edition (New York: Garland Science Publishing)

Janosov M, Virágh C, Vásárhelyi G and Vicsek T 2017 Group chasing tactics: how to catch a faster prey *New J. Phys.* **19** 053003

Jin W, McCue S W and Simpson M J 2018 Extended logistic growth model for heterogeneous populations *J. Theor. Biol.* **445** 51–61

Johnston S T, Baker R E and Simpson M J 2017 A new and accurate continuum description of moving fronts *New J. Phys.* **19** 033010

Keeley P W, Zhou C, Lu L, Williams R W, Melmed S and Reese B E 2014 Pituitary tumor-transforming gene 1 regulates the patterning of retinal mosaics *Proc. Natl. Acad. Sci. USA* **111** 9295–00

Lambert G, Bergman A, Zhang Q, Bortz D and Austin R 2014 Physics of biofilms: the initial stages of biofilm formation and dynamics *New J. Phys.* **16** 045005

Law R and Dieckmann U 2000 A dynamical system for neighbourhoods in plant communities *Ecology* **81** 2137–48

Law R, Murrell D J and Dieckmann U 2003 Population growth in space and time: Spatial logistic equations *Ecology* **84** 252–62

Lukeman R, Li Y and Edelstein-Keshet L 2010 Inferring individual rules from collective behavior *Proc. Natl. Acad. Sci. USA* **107** 12576–80

Murrell D J and Law R 2003 Heteromyopia and the spatial coexistence of similar competitors *Ecol. Lett.* **6** 48–59

Murrell D J, Dieckmann U and Law R 2004 On moment closures for population dynamics in continuous space *J. Theor. Biol.* **229** 421–32

Newman T J and Grima R 2004 Many-body theory of chemotactic cell-cell interactions *Phys. Rev. E* **70** 051916

Oliveira S, Rosowski E E and Huttenlocher A 2016 Neutrophil migration in infection and wound repair: going forward in reverse *Nat. Rev. Immunol.* **16** 378–91

Oshanin G, Vasilyev O, Krapivsky P L and Klafter J 2009 Survival of an evasive prey *Proc. Natl. Acad. Sci. USA* **106** 13696–01

Plank M J and Simpson M J 2012 Models of collective cell behaviour with crowding effects: comparing lattice based and lattice-free approaches *J. R. Soc. Interface* **9** 2983–96

Plank M J and Law R 2015 Spatial point processes and moment dynamics in the life sciences: A parsimonious derivation and some extensions *Bull. Math. Biol.* **77** 586–13

Raghib M, Hill N A and Dieckmann U 2011 A multiscale maximum entropy moment closure for locally

regulated space-time point process models of population dynamics *J. Math. Biol.* **62** 605–53

Raz E and Mahabaleshwar H 2009 Chemokine signaling in embryonic cell migration: a fisheye view *Development* **136** 1223–29

Sharkey K J, Fernandez C, Morgan K L, Peeler E, Thrush M, Turnbull J F and Bowers R 2006 Pair-level approximations to the spatio-temporal dynamics of epidemics on asymmetric contact networks *J. Math. Biol.* **53** 61–85

Simpson M J, Landman K A and Hughes B D 2009 Multi-species simple exclusion processes *Physica A* **388** 399–06

Smith C A and Yates C A 2018 Spatially extended hybrid methods: a review *J. R. Soc. Interface* **15** 20170931

Surendran A, Plank M J and Simpson M J 2018 Spatial moment description of birth-death-movement processes incorporating the effects of crowding and obstacles *Bull. Math. Biol.* **80** 2828–55

Tambe D T, Hardin C C, Angelini T E, Rajendran K, Park C Y, Serra-Picamal X, Zhou E H, Zaman M H, Butler J P, Weitz D A, Fredberg J J and Trepat X 2011 Collective cell guidance by cooperative intercellular forces *Nat. Mater.* **10** 469–75

Thomas R J, Bennett A, Thomson B and Shakesheff K M 2006 Hepatic stellate cells on ploy(DL-lactic acid) surfaces control the formation of 3D hepatocyte co-culture aggregates in vitro *Eur. Cell Mater.* **11** 16–26

Vicsek T 2010 Closing in on evaders *Nature* **466** 43–44

Williams M L K and Solnica-Krezel L 2017 Regulation of gastrulation movements by emergent cell and tissue interactions *Curr. Opin. Cell Biol.* **48** 33–39

Wolf K and Friedl P 2011 Extracellular matrix determinants of proteolytic and non-proteolytic cell migration *Trends Cell Biol.* **21** 736–744

Yang S, Jiang S, Jiang L, Li G and Han Z 2014 Aggregation increases prey survival time in group chase and escape *New J. Phys.* **16** 083006